The American Journal of Pathology, Vol. 189, No. 4, April 2019

The American Journal of
PATHOLOGY
ajp.amjpathol.org

GASTROINTESTINAL, HEPATOBILIARY, AND PANCREATIC PATHOLOGY

β1 Syntrophin Supports Autophagy Initiation and Protects against Cerulein-Induced Acute Pancreatitis

Risheng Ye,*† Toshiharu Onodera,* Pierre-Gilles Blanchard,* Christine M. Kusminski,* Victoria Esser,‡ Rolf A. Brekken,§¶ and Philipp E. Scherer*

From the Touchstone Diabetes Center, Department of Internal Medicine, the Departments of Biophysics‡ and Surgery,¶ and the Hamon Center for Therapeutic Oncology Research,§ University of Texas Southwestern Medical Center, Dallas; and the Department of Medical Education,† Texas Tech University Health Sciences Center Paul L. Foster School of Medicine, El Paso, Texas*

Accepted for publication January 2, 2019.

Address correspondence to Philipp E. Scherer, Ph.D., Touchstone Diabetes Center, Department of Internal Medicine, University of Texas Southwestern Medical Center, 5323 Harry Hines Blvd., Dallas, TX 75390-8549. E-mail: philipp.scherer@utsouthwestern.edu.

Syntrophins are a family of proteins forming membrane-anchored scaffolds and serving as adaptors for various transmembrane and intracellular signaling molecules. To understand the physiological roles of β1 syntrophin, one of the least characterized members, we generated mouse models to eliminate β1 syntrophin specifically in the endocrine or exocrine pancreas. β1 syntrophin is dispensable for the morphology and function of insulin-producing β cells. However, mice with β1 syntrophin deletion in exocrine acinar cells exhibit increased severity of cerulein-induced acute pancreatitis. Reduced expression of cystic fibrosis transmembrane conductance regulator and dilation of acinar lumen are potential predisposition factors. During the disease progression, a relative lack of autophagy is associated with deficiencies in both actin assembly and endoplasmic reticulum nucleation. Our findings reveal, for the first time, that β1 syntrophin is a critical regulator of actin cytoskeleton and autophagy in pancreatic acinar cells and is potently protective against cerulein-induced acute pancreatitis. *(Am J Pathol 2019, 189: 813–825; https://doi.org/10.1016/j.ajpath.2019.01.002)*

Acute pancreatitis is a life-threatening disease characterized by necrotic inflammation of the exocrine pancreas.[1] The pathologic findings include parenchymal edema, neutrophil infiltration, pancreatic acinar cell vacuolization and necrosis, as well as a prominent elevation of blood amylase and lipase. Acute pancreatitis has a variety of etiologies, with the primary contributors being gallstones and alcohol abuse. Autoactivation of trypsin and subsequently other digestive enzymes within the acinar cells contributes to cell death and noxious leakage. However, the molecular mechanisms underlying the pathogenesis of acute pancreatitis remain to be better defined.

Cerulein is a 10–amino acid peptide analog to cholecystokinin. Supraphysiological doses of cerulein have been used extensively to induce experimental acute pancreatitis in rodents.[2] Cerulein-induced acute pancreatitis is reversible and recapitulates the aforementioned pathologic features in humans, including intracellular activation of digestive enzymes in acinar cells. Moreover, an hourly injection protocol of cerulein administration allows fine-tuning of the severity and pathogenic stage of pancreatitis, which is advantageous for mechanistic studies.

Syntrophins are a family of perimembrane scaffolding proteins with five members in mammals, α (acidic) 1, β (basic) 1, β (basic) 2, γ1, and γ2.[3] γ1 And γ2 syntrophins were reported to locate in the endoplasmic reticulum (ER) of neurons and skeletal muscle cells.[4] In contrast, syntrophins α1, β1, and β2 bind to cytoplasmic dystrophin-associated

Supported by NIH grants R01-DK55758, R01-DK099110, and P01-DK088761-01; JDRF grant 2-SRA-2016-149-Q-R; a Novo Nordisk Research Foundation unrestricted grant (P.E.S.); a Naomi Berrie Diabetes Center, Columbia University Medical Center, research fellowship (R.Y.); and Merck Sharp & Dohme Life Science Foundation and Mochida Memorial Foundation for Medical and Pharmaceutical Research, Japan (T.O.).

Disclosures: None declared.

https://doi.org/10.1016/j.ajpath.2019.01.002

protein complexes, which are defective in major human congenital muscular dystrophies.[5] These three cytoplasmic syntrophins recruit transmembrane Na^+ and K^+ channels[6,7] as well as G proteins[3] in neurons or muscles cells. α1 Syntrophin interacts with F-actin and the cytoskeleton.[8] β2 Syntrophin modulates the exocytosis of insulin granules in an INS-1 β-cell line.[9,10] However, the physiological roles of β1 syntrophin are poorly understood. Herein, we report the generation of inducible, tissue-specific knockout mouse models of β1 syntrophin. Ablation of β1 syntrophin in pancreatic β cells did not cause apparent changes to β-cell morphology or function. However, mice harboring a β1 syntrophin knockout in the exocrine pancreatic acinar cells showed diminished expression of cystic fibrosis transmembrane conductance regulator (CFTR) as well as dilation of acinar lumina. They were more susceptible to cerulein-induced acute pancreatitis, associated with reduced autophagic activity and massive disruption of secretory granules. The autophagy deficiency can be mainly attributed to the early steps (ie, actin assembly and ER curvature). Collectively, we unravel novel and significant roles of β1 syntrophin in pancreatic acinar cells, including actin organization, autophagy initiation, and protection against cerulein-induced acute pancreatitis.

Materials and Methods

Mice

The *Sntb1*-targeted ($Sntb1^{T/T}$) mouse strain was derived from the embryonic stem cell clone (EPD0463_5_C05; European Conditional Mouse Mutagenesis Program, Neuherberg, Germany) with the assistance of the University of Texas Southwestern Medical Center (UTSW) Transgenic Core. The *Sntb1*-floxed ($Sntb1^{F/F}$) mouse strain was generated by crossing $Sntb1^{T/T}$ with the transgenic strain *actin-Flp* (003800; Jackson Laboratory, Bar Harbor, ME). *Ptf1a-rtTA* (pancreas-associated transcription factor 1a—reverse tetracycline-controlled transactivator; 018070) and *TRE-Cre* (006234) were purchased from the Jackson Laboratory. *MIP-rtTA* was generated and characterized by the Scherer laboratory.[11,12] *Ptf1a-Cre* was obtained from the Brekken laboratory and maintained in the FVB genetic background, whereas all of the other original strains were bred in the C57BL/6 genetic background. *Sntb1-βKO* (*MIP-rtTA*; *TRE-Cre*; $Sntb1^{F/F}$) mice were controlled by their *MIP-rtTA*; $Sntb1^{F/F}$ and $Sntb1^{F/F}$ littermates. *Sntb1-acKO* (*Ptf1a-Cre*; $Sntb1^{F/F}$) mice were maintained in a mixed genetic background of FVB and C57BL/6 through sibling matings and controlled by their $Sntb1^{F/F}$ and *Ptf1a-Cre* littermates. Mice were housed on a 12-hour dark/light cycle, with ad libitum access to water and diet. Diets used in this study include regular chow diet (5058; LabDiet, St. Louis, MO) and doxycycline chow diet (S7123, 600 mg/kg; Bio-Serv, Flemington, NJ). All protocols for mouse use and euthanasia were reviewed and approved by the Institutional Animal Care and Use Committee of UTSW.

Genotyping PCR

Approximately 2 mm of mouse tail tip was incubated in 80 μL 50 mmol/L NaOH at 95°C for 1.5 hours. Tris-HCl (pH 8.0; 1 mol/L; 8 μL) was added for neutralization. After vortex mixing and a short spin down, 1 μL of supernatant was used as a PCR template. Primer pairs for genotyping PCR were as follows: 5′-GGGGGTACCGCGTCGAGAAGTTC-3′ (forward) and 5′-GCAGTTACAGAGATCTGCAGCTTGCCC-3′ (reverse) for *Sntb1*-targeted allele; 5′-GTTGAGAGTAAGGCGCATAAC-GATACCACG-3′ (forward) and 5′-GCAGTTACAGA-GATCTGCAGCTTGCCC-3′ (reverse) for *Sntb1*-floxed allele; 5′-GCTACTTTCATCAATTGTGGAAGATTCAGCG-3′ (forward) and 5′-CACAACATTAGTCAACTCCGTTA-GGCCC-3′ (reverse) for *actin-Flp*; 5′-GATTTCGAC-CAGGTTCGTTCACTCA-3′ (forward) and 5′-GCTAAC-CAGCGTTTTCGTTCTGCCA-3′ (reverse) for *TRE-Cre*; 5′-GTGGATGTAGTTATAAGAATCCTCGCGTGCC-3′ (forward) and 5′-CCAGTACAGGGTAGGCTGCTCAACTCC-3′ (reverse) for *Ptf1a-rtTA*; and 5′-CACCTGGAGACCTTAAT-GGGCCAAAC-3′ (forward) and 5′-CGATTGGCAGGG-CATCGAGC-3′ (reverse) for *MIP-rtTA*. The PCR program was as follows: 95°C for 5 minutes, followed by 35 cycles of 95°C for 15 seconds, 62°C for 30 seconds, and 72°C for 30 seconds, and ending with 72°C for 3 minutes.

Western Blot Analysis

Protein lysates were prepared from mouse pancreata and subjected to Western blot analysis, as previously described.[13] Primary antibodies included β1 syntrophin (sc-13763; Santa Cruz Biotechnology, Santa Cruz, CA), glyceraldehyde-3-phosphate dehydrogenase (2118; Cell Signaling, Danvers, MA), β-actin (NB600-501; Novus, Littleton, CO), α1 syntrophin (ab188873; Abcam, Cambridge, MA), β2 syntrophin (MA1-745; Thermo Fisher, Waltham, MA), autophagy-related 9A (ATG9A; ab108338; Abcam), p62 (5114; Cell Signaling), and light chain 3 (LC3; PM036; MB, Des Plaines, IL). Immunoblots were imaged on an Odyssey CLx infrared imaging system (LI-COR, Lincoln, NE) and quantitated with ImageJ version 1.45h (NIH, Bethesda, MD; http://imagej.nih.gov/ij) Gel Analyzer.

Immunofluorescence

Mouse pancreata were harvested and processed for paraffin sections, as previously described.[12] Primary antibodies used for immunofluorescence were β1 syntrophin (sc-13763; Santa Cruz Biotechnology), insulin (A0564; Dako, Carpinteria, CA), CFTR (NB300-511; Novus), NF-κB p65 (4764; Cell Signaling), LC3 (PM036; MBL), β-actin (3700; Cell Signaling), and α-tubulin (62204; Thermo Fisher). DAPI (D9542, 300 nmol/L; Sigma-Aldrich, St. Louis, MO) was

used for counterstaining. Images were acquired on a Zeiss Axio Observer Z1 inverted microscope (Zeiss, Oberkochen, Germany) or a Keyence BZ-X710 fluorescence microscope (Keyence America, Itasca, IL), and they were quantitated with ImageJ software.

Glucose Tolerance Test

Mice were fasted for 4 to 6 hours and subjected to an oral gavage of dextrose (1 mg/g body weight). Tail blood was measured for glucose at 0, 15, 60, and 120 minutes with a Contour glucose meter (82486543; Bayer, Pittsburgh, PA).

Transmission Electron Microscopy and Quantitation

Under isoflurane anesthesia, mice were subjected to cardiac perfusion of a perfusion buffer (4% paraformaldehyde, 1% glutaraldehyde, and 0.1 mol/L sodium cacodylate, pH 7.4). Pancreata were dissected, transferred to fixative (2.5% glutaraldehyde and 0.1 mol/L sodium cacodylate, pH 7.4), minced to <1-mm pieces, and then processed at the UTSW Electron Microscopy Core Facility. Sections were examined with a JEOL 1200 EX electron microscope (JOEL USA, Peabody, MA) and imaged with a SIS Morada 11 Mega-Pixel side-mounted charge-coupled device camera (EMSIS, Münster, Germany). Interested areas were selected and quantitated with Adobe Photoshop 7.0 (Adobe Systems, San Jose, CA) and ImageJ software.

Cerulein-Induced Acute Pancreatitis

Mice were subjected to consecutive hourly i.p. injections of cerulein (C9026; Sigma-Aldrich) at a dosage of 50 μg/kg body weight per injection. Cerulein solution [10 mg/L phosphate-buffered saline (PBS)] was injected at the volume of 5 mL/kg body weight. The same volume of PBS was injected into the vehicle-treated groups. One hour after the last injection, mice were euthanized and collected for tissues.

Lysosomal Inhibition

Mice were subjected to an i.p. injection of chloroquine (C6628; Sigma-Aldrich) at a dosage of 0.1 g/kg body weight. Chloroquine solution (20 g/L PBS) was injected at the volume of 5 mL/kg body weight. The same volume of PBS was injected into the vehicle-treated groups. Mice were euthanized and collected for tissues 1.5 hours after the chloroquine administration.

Serum Digestive Enzymes

Mouse blood was collected from the facial vein and prepared for serum. Serum samples were assayed for amylase and trypsin on a Vitros 250 chemistry analyzer (Johnson & Johnson, New Brunswick, NJ) at the UTSW Mouse Metabolic Phenotyping Core.

Histologic Analysis and Quantitation

Mouse pancreata were processed for paraffin sections and hematoxylin and eosin staining at the UTSW Molecular Pathology Core. Images were acquired on an Olympus FSX100 microscope (Olympus Scientific Solutions, Waltham, MA) with a 20× objective. Total acinar cell number was quantitated with ImageJ software. Acinar cells with necrosis or vacuoles, as well as peripancreatic neutrophils, were identified, as previously described,[14] counted with ImageJ software, summed, and normalized against the total acinar cells examined in an individual mouse. For edema quantitation, whole hematoxylin and eosin−stained pancreas sections were scanned on an Epson Expression 10000 XL photo scanner (Epson America, Long Beach, CA) at a resolution of 2400 dots per inch, as previously described.[13] Both peripancreatic nonparenchymal space and total pancreas area were quantitated with Adobe Photoshop 7.0, summed for individual mice, and calculated for percentage. The histologic characteristics were evaluated by an expert experienced in the mouse pathology of acute pancreatitis (R.Y.).

TUNEL Assay and Quantitation

Terminal deoxynucleotidyl transferase-mediated dUTP nick-end labeling (TUNEL) assays on paraffin sections were performed with the *in situ* cell death detection kit, TMR red (12156792910; Roche, Indianapolis, IN), and counterstained with 300 nmol/L DAPI. Images were acquired on a Zeiss Axio Observer Z1 inverted microscope. Quantitation of TUNEL-positive cell percentage was performed with ImageJ software, as previously described.[15]

Caspase-3 Activity Assay

Caspase-3 activity in mouse pancreas was measured with a colorimetric kit (ab39401; Abcam) and normalized against the protein content assayed by a bicinchoninic acid kit (23225; Thermo Scientific, Waltham, MA).

Amylase Secretion Assay

Amylase secretion from freshly isolated acini was measured, as previously described.[16] Briefly, mouse exocrine pancreas was digested by common bile duct injection of 0.2 g/L Liberase TL (05401020001; Roche) in incubation solution, which is composed of Dulbecco's modified Eagle's medium (D5796; Sigma-Aldrich), 0.1 g/L soybean trypsin inhibitor (T9003; Sigma-Aldrich), and 0.1% bovine serum albumin. After incubation at 37°C in a water bath for 40 minutes, acini were dispersed by a brief vortex, harvested from supernatants, and rinsed with incubation solution. The isolated acini were resuspended with 25 mL incubation solution per

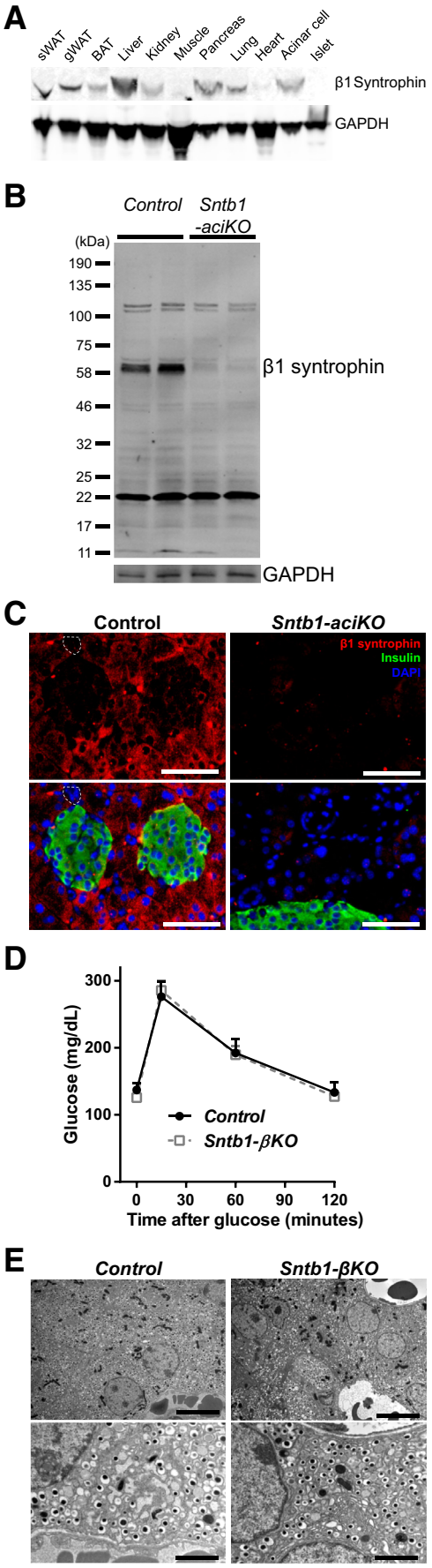

mouse and evenly distributed into 1-mL aliquots. Cerulein stock solutions (200×) were added to the aliquots to reach a working concentration of 0, 1, 3, 10, 30, 100, 1000, 10,000, or 100,000 pmol/L. After incubation at 37°C in a water bath shaker (60 rpm) for 30 minutes, acini-free medium was sampled from the aliquots and assayed for amylase secretion, which was normalized against the protein content of the corresponding acini pellets, and then calculated as percentage of the total amylase content determined from the aliquots treated with 0 pmol/L cerulein.

Statistical Analysis

Two-tailed *t*-test was applied for all pairwise comparisons unless otherwise indicated. Statistical significance was accepted at $P < 0.05$.

Results

Conditional Knockout of β1 Syntrophin in Mice

β1 Syntrophin expression was first surveyed in various mouse tissues by using Western blot analysis (Figure 1A). The abundant levels of β1 syntrophin in the pancreas are mainly contributed by the exocrine acinar cells, whereas the endocrine islets of Langerhans only express a marginal level.

To investigate the physiological functions of β1 syntrophin, embryonic stem cell clones were obtained with *Sntb1*-targeted mutation from the European Conditional Mouse Mutagenesis Program. The targeted mutation used the knockout-first strategy[17] [ie, in the targeted allele (*tm1a*) of the *Sntb1* gene, reporter cassettes were inserted into the intron to disrupt the gene expression] (Supplemental Figure S1A). Mice homozygous in the *Sntb1*-targeted alleles ($Sntb1^{T/T}$) were derived from the embryonic stem cells. Western blot analysis revealed that the expression of β1 syntrophin was partially reduced in the $Sntb1^{T/T}$ mice (Supplemental Figure S1B).

To generate a mouse strain enabling conditional elimination of β1 syntrophin, the $Sntb1^{T/T}$ mice were crossed with actin-*Flp* transgenic mice to remove the reporter

Figure 1 Normal β-cell structure and function in *Sntb1-βKO* mice. **A:** Western blot analysis of β1 syntrophin in the indicated tissues from wild-type mice. An equal amount of 71 μg protein was loaded per lane. Glyceraldehyde-3-phosphate dehydrogenase (GAPDH) was also blotted as reference. **B** and **C:** $Sntb1^{F/F}$ (control) and *Ptf1a-rtTA; TRE-Cre;* $Sntb1^{F/F}$ (*Sntb1-aciKO*) mice were fed a doxycycline chow diet for 2 weeks and harvested for pancreata. **B:** Western blot analysis of β1 syntrophin. **C:** Immunofluorescence of β1 syntrophin (red) and insulin (green), and counterstaining of DAPI (blue). **Top row:** β1 Syntrophin signal only. **Bottom row:** Signal merged with insulin and DAPI. **Dashed lines** indicate small ducts. **D** and **E:** *MIP-rtTA; TRE-Cre;* $Sntb1^{F/F}$ (*Sntb1-βKO*) and $Sntb1^{F/F}$ (control) mice were fed a doxycycline chow diet for 2 weeks. **D:** Blood glucose during a glucose tolerance test. **E:** Representative transmission electron microscopy images of β cells. Data are expressed as means ± SEM (**D**). $n = 6$ control (**D**); $n = 8$ *Sntb1-βKO* (**D**). Scale bars: 50 μm (**C**); 2 μm (**E**, **top row**); 0.4 μm (**E**, **bottom row**). BAT, brown adipose tissue; gWAT, gonadal white adipose tissue; sWAT, s.c. white adipose tissue.

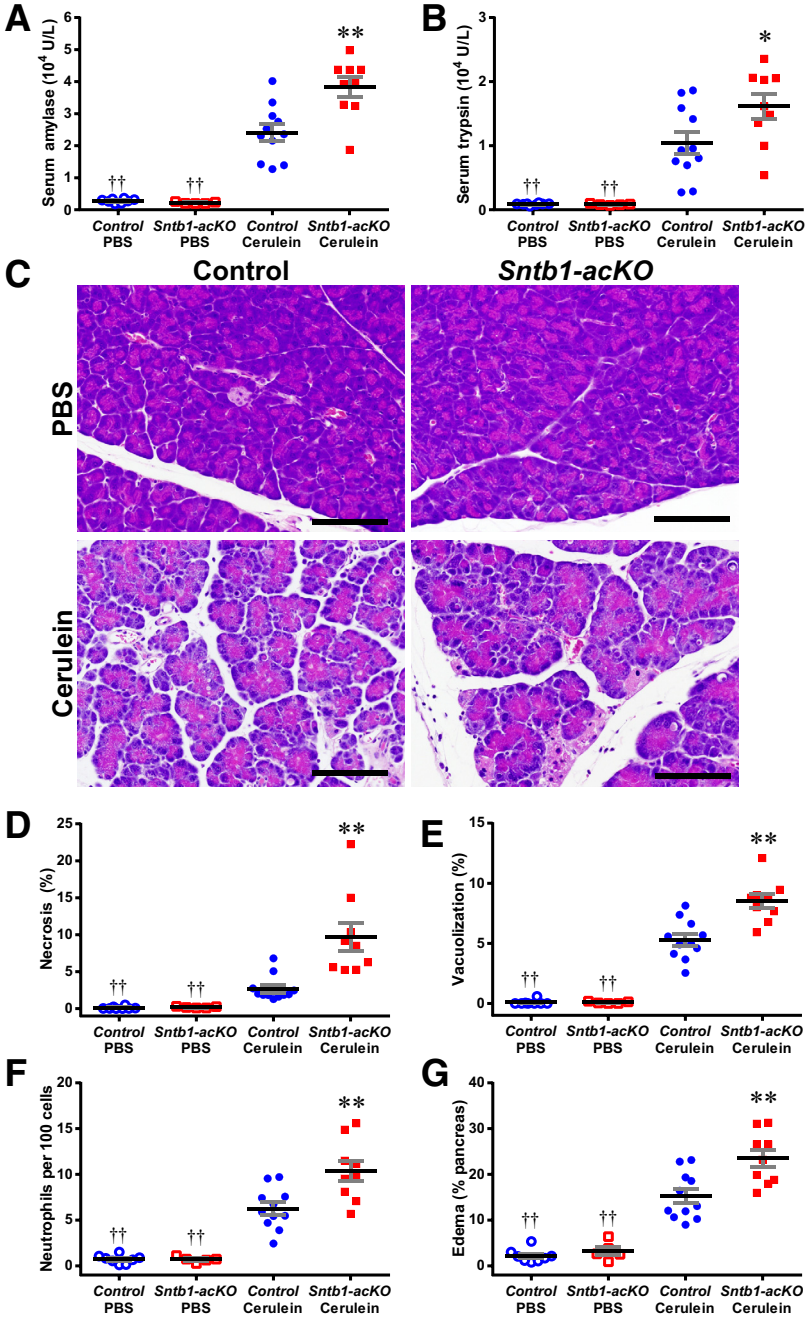

Figure 2 Exacerbated experimental acute pancreatitis in *Sntb1-acKO* mice. *Sntb1-acKO* (*Ptf1a-Cre*; *Sntb1*$^{F/F}$) and control (*Ptf1a-Cre* or *Sntb1*$^{F/F}$) mice were subjected to seven consecutive hourly i.p. injections of cerulein (50 μg/kg body weight) or phosphate-buffered saline (PBS), followed by euthanasia and tissue harvest. **A** and **B:** Serum levels of digestive enzymes amylase (**A**) and trypsin (**B**). **C:** Representative hematoxylin and eosin staining images of pancreas. **D** and **E:** Percentages of necrotic (**D**) and vacuolized (**E**) acinar cells. **F** and **G:** Peripancreatic neutrophils, normalized against the number of acinar cells (**F**), and nonparenchymal space, normalized against the area of pancreas (**G**). Dots represent individual mice. Data are expressed as means ± SEM (**A**, **B**, and **D**–**G**). $n = 8$ PBS-treated control (**A**, **B**, and **D**–**G**); $n = 5$ PBS-treated *Sntb1-acKO* (**A**, **B**, and **D**–**G**); $n = 11$ cerulein-treated control (**A**, **B**, and **D**–**G**); $n = 9$ cerulein-treated *Sntb1-acKO* (**A**, **B**, and **D**–**G**). $^{*}P < 0.05$, $^{**}P < 0.01$ versus control mice; $^{\dagger\dagger}P < 0.01$ cerulein versus PBS treatment. Scale bar = 0.1 mm (**C**).

cassettes in the *Sntb1*-targeted allele, rendering the *Sntb1* into a floxed allele configuration (Supplemental Figure S1, A and C). By crossing the *Sntb1*$^{F/F}$ strain with the *Ptf1a-rtTA* and *TRE-Cre* transgenics, followed by doxycycline treatment (*Sntb1-aciKO*) (Supplemental Figure S1D), nearly complete elimination of β1 syntrophin protein was observed in pancreatic acinar cells by using Western blot analysis (Figure 1B). Immunofluorescence confirms the differential expression of β1 syntrophin in acinar and islet cells of control mice and the depletion of β1 syntrophin in the exocrine pancreas of *Sntb1-aciKO* mice (Figure 1C). This validates the functionality of the *Sntb1*$^{F/F}$ strain for the purpose of eliminating *Sntb1* in specific cell types. The expression levels of β1 syntrophin in wild-type mice are low in small ductal cells compared with the acinar cells.

Ablation of β1 Syntrophin Does Not Affect β-Cell Morphology and Function

To determine whether β1 syntrophin is critical in the insulin-producing β cells of the endocrine pancreas, the *Sntb1*$^{F/F}$ strain was crossed with the transgenic strains *MIP-rtTA* and *TRE-Cre* (Supplemental Figure S1E), to generate the *Sntb1-βKO* mouse model. After doxycycline-induced

knockout of *Sntb1* in β cells, *Sntb1-βKO* mice exhibit normal fasting glucose and oral glucose tolerance (Figure 1D). By transmission electron microscopy, no apparent abnormality is observed in the intracellular morphology of their β cells (Figure 1E). These data suggest that loss of β1 syntrophin does not affect β-cell function under normal conditions.

β1 Syntrophin Protects against Cerulein-Induced Acute Pancreatitis

To investigate the function of β1 syntrophin in the exocrine pancreas, the *Sntb1-acKO* mice were generated by crossing the $Sntb1^{F/F}$ strain with the *Ptf1a-Cre* transgenic strain (Supplemental Figure S1F), and *Sntb1* was deleted in adult acinar, ductal, and pre-endocrine cells.[18] *Sntb1-acKO* mice appeared normal without an obvious baseline phenotype. However, we wanted to test if β1 syntrophin would help acinar cells to cope with pathologic stresses, such as acute pancreatitis. *Sntb1-acKO*, $Sntb1^{F/F}$, and *Ptf1a-Cre* mice were subjected to seven consecutive hourly i.p. injections of cerulein to induce acute pancreatitis.[14] The latter two control genotypes with intact *Sntb1* expression exhibited similar phenotypes without any statistically significant differences (data not shown), and they were combined into one group of control mice. As the primary diagnostic metrics of acute pancreatitis, serum levels of the active digestive enzymes amylase ($3.8 \pm 0.3 \times 10^4$ U/L versus $2.4 \pm 0.3 \times 10^4$ U/L; $P = 0.002$) (Figure 2A) and trypsin ($1.6 \pm 0.2 \times 10^4$ U/L versus $1.0 \pm 0.2 \times 10^4$ U/L; $P = 0.04$) (Figure 2B) were significantly increased (by >50%) in *Sntb1-acKO* mice compared with controls. Meanwhile, the levels of these enzymes in the vehicle (PBS)−treated groups were marginal.

The severity of acute pancreatitis was further characterized by pathologic analyses. Compared with the PBS-treated group, cerulein-treated animals displayed marked increases in cell necrosis and vacuolization and neutrophil infiltration, as well as an increase in the peripancreatic nonparenchymal space, an indicator of edema (Figure 2C). Between the two cerulein-treated groups, *Sntb1-acKO* mice show a 3.6-fold increase (9.7% ± 1.9% versus 2.7% ± 0.5%; $P = 0.006$) in cell necrosis (Figure 2D), a 1.6-fold increase (8.5% ± 0.6% versus 5.3% ± 0.5%; $P = 0.0005$) in vacuolized cells (Figure 2E), a 1.7-fold increase (10.4 ± 1.1 per 100 acinar cells versus 6.3 ± 0.7 per 100 acinar cells; $P = 0.004$) in infiltrating neutrophils (Figure 2F), and a 1.5-fold increase (23% ± 2% versus 15% ± 2%; $P = 0.003$) in nonparenchymal space (Figure 2G), compared with control mice. The nuclear localization of the p65 NF-κB subunit is similar between these two genotypes (1.0% ± 0.1% versus 1.1% ± 0.1%; $P = 0.86$) (Supplemental Figure S2, A and B), not supporting a role of NF-κB−mediated inflammatory signaling as a major driving force for the phenotypic differences. A significance difference in DNA breakage of acinar cells (3.1% ± 0.7% versus 3.9% ± 1.0%; $P = 0.48$), as judged by TUNEL assays (Supplemental Figure S2, C and D), was also not observed. *Sntb1-acKO* mice display higher caspase-3 activity in pancreas tissue than control mice after three hourly injections of cerulein, but not at the other measured time points (0, 1, 2, 5, and 7 hourly injections) (Supplemental Figure S2E). Combined, all these pathologic parameters consistently indicate a more necrotic microenvironment, cell damage, and enhanced inflammation in *Sntb1-acKO* mice, suggesting a protective role of β1 syntrophin in experimental acute pancreatitis.

β1 Syntrophin Regulates Acinar Lumen Size and CFTR Expression

To understand the cellular mechanisms underlying the protective role of β1 syntrophin in experimental acute pancreatitis, transmission electron microscopy was used to examine the morphology of the exocrine pancreas from mice after four hourly injections of cerulein or PBS. In PBS-treated animals, *Sntb1* ablation leads to an overall increase (3.8-fold, $P = 0.00003$) in the size of acinar lumina (Figure 3A), where the digestive zymogens and mucus are secreted from acinar cells and collected into pancreatic ducts.

Because the dilation of pancreatic lumina and ducts is often associated with mucus accumulation due to defects in ion channels, such as CFTR,[19] CFTR expression was examined in the pancreas of PBS-treated animals by immunofluorescence (Figure 3, B−D). Interestingly, *Sntb1-acKO* mice exhibit significantly weaker CFTR signals in acinar (Figure 3B) and ductal (Figure 3C) cells, but not in the islets of Langerhans (Figure 3D). CFTR deficiency is known to increase luminal mucus accumulation and pancreatic ductal dilation, and it eventually leads to fibrosis and chronic pancreatitis.[20] Therefore, the CFTR reduction in *Sntb1-acKO* exocrine pancreas may be a predisposing factor for the severity of acute pancreatitis. As for the capacity in amylase secretion, a statistically significant difference between the two genotypes was not detected when isolated acini were stimulated with a range of cerulein concentrations, ranging from basal (1 pmol/L) to supraphysiological (100 nmol/L) levels (Figure 3E). Taken together, it is possible that the amorphous electron-dense material in the dilated acinar lumen of *Sntb1-acKO* mice is mainly composed of insoluble debris rather than digestive enzymes.

β1 Syntrophin Is Required for Autophagy during Cerulein-Induced Acute Pancreatitis

In the acinar cells of cerulein-treated control mice, a dramatic occurrence of autophagy (Figure 4, A and B) was observed, including different stages of autophagosome (Supplemental Figure S3A) and autolysosome (Supplemental Figure S3B) formation. In striking contrast, autophagy was rare when β1 syntrophin was absent (Figure 4, A and B, and Supplemental Figure S3, C and D). Instead, secretory granules with disrupted membranes and contents that leak into the cytosol are

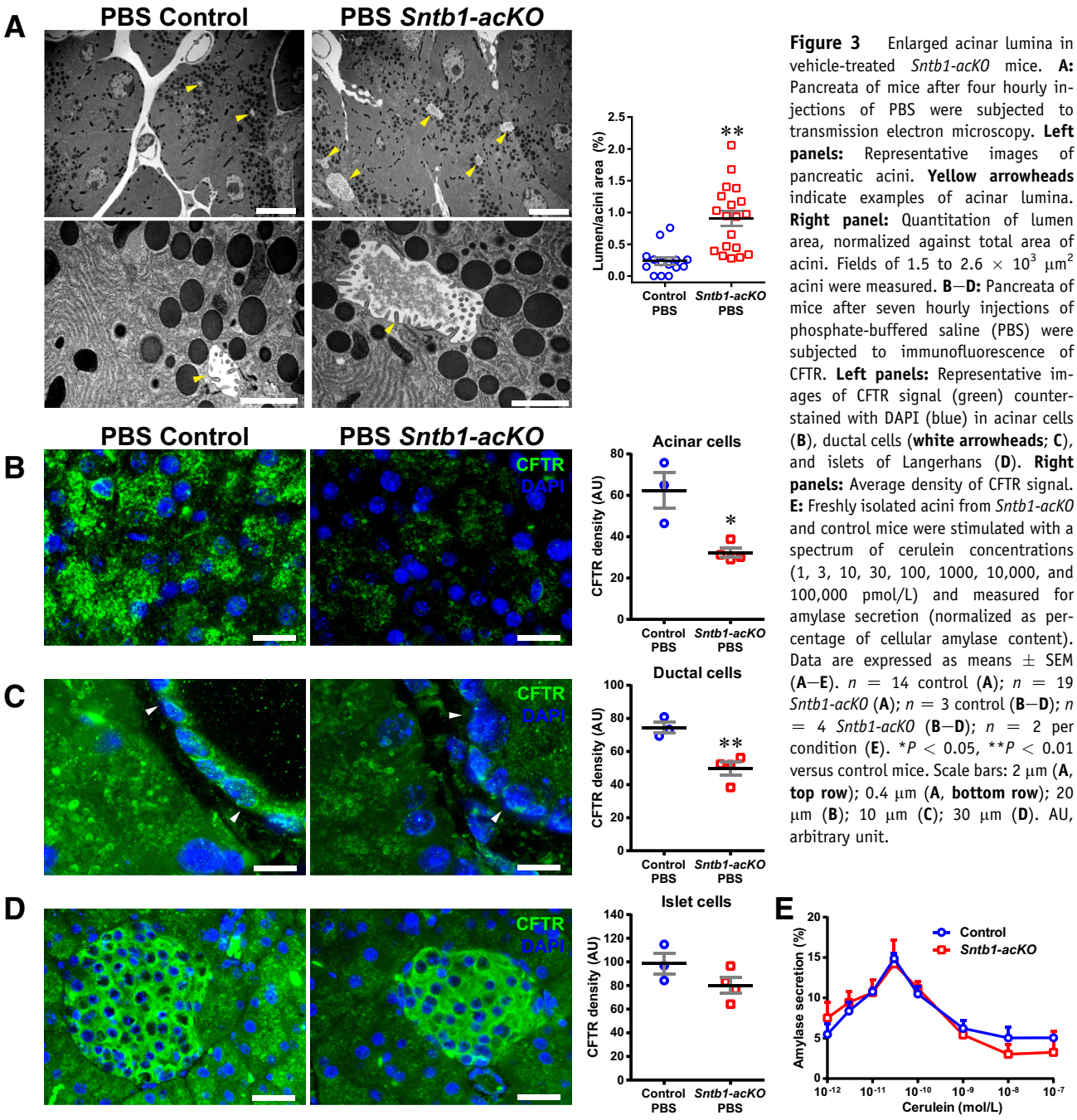

Figure 3 Enlarged acinar lumina in vehicle-treated *Sntb1-acKO* mice. **A:** Pancreata of mice after four hourly injections of PBS were subjected to transmission electron microscopy. **Left panels:** Representative images of pancreatic acini. **Yellow arrowheads** indicate examples of acinar lumina. **Right panel:** Quantitation of lumen area, normalized against total area of acini. Fields of 1.5 to 2.6 × 10^3 μm^2 acini were measured. **B**—**D:** Pancreata of mice after seven hourly injections of phosphate-buffered saline (PBS) were subjected to immunofluorescence of CFTR. **Left panels:** Representative images of CFTR signal (green) counterstained with DAPI (blue) in acinar cells (**B**), ductal cells (**white arrowheads**; **C**), and islets of Langerhans (**D**). **Right panels:** Average density of CFTR signal. **E:** Freshly isolated acini from *Sntb1-acKO* and control mice were stimulated with a spectrum of cerulein concentrations (1, 3, 10, 30, 100, 1000, 10,000, and 100,000 pmol/L) and measured for amylase secretion (normalized as percentage of cellular amylase content). Data are expressed as means ± SEM (**A**—**E**). n = 14 control (**A**); n = 19 *Sntb1-acKO* (**A**); n = 3 control (**B**—**D**); n = 4 *Sntb1-acKO* (**B**—**D**); n = 2 per condition (**E**). $^*P < 0.05$, $^{**}P < 0.01$ versus control mice. Scale bars: 2 μm (**A**, **top row**); 0.4 μm (**A**, **bottom row**); 20 μm (**B**); 10 μm (**C**); 30 μm (**D**). AU, arbitrary unit.

ubiquitously found in *Sntb1*-knockout acinar cells (Figure 4A). These data suggest that autophagy is an adaptive response during cerulein-induced acute pancreatitis, and β1 syntrophin is required for the autophagic process. In the absence of β1 syntrophin and autophagy, more autoactivated digestive enzymes are released into the cytosol and accelerate cell necrosis. Interestingly, β1 syntrophin protein in control pancreas is significantly diminished after cerulein treatment (Figure 4, C and D), which could be attributed to both the autoactivated digestive enzymes and the autophagic degradation. Depletion of β1 syntrophin does not induce compensatory up-regulation of α1 or β2 syntrophin (Figure 4, C, E, and F).

Autophagy marker proteins were examined at different stages.[21] ATG9 delivers cell membranes to the expanding phagophore, and it is dramatically reduced after hourly cerulein injections in both control and *Sntb1-acKO* mice (Figure 5, A and B). The ATG9A protein levels display a partial recovery at the time point of 2 hours and remain significantly lower than the untreated ones. The cargo protein p62, which targets the cellular proteins to autophagosomes, also exhibits an initial

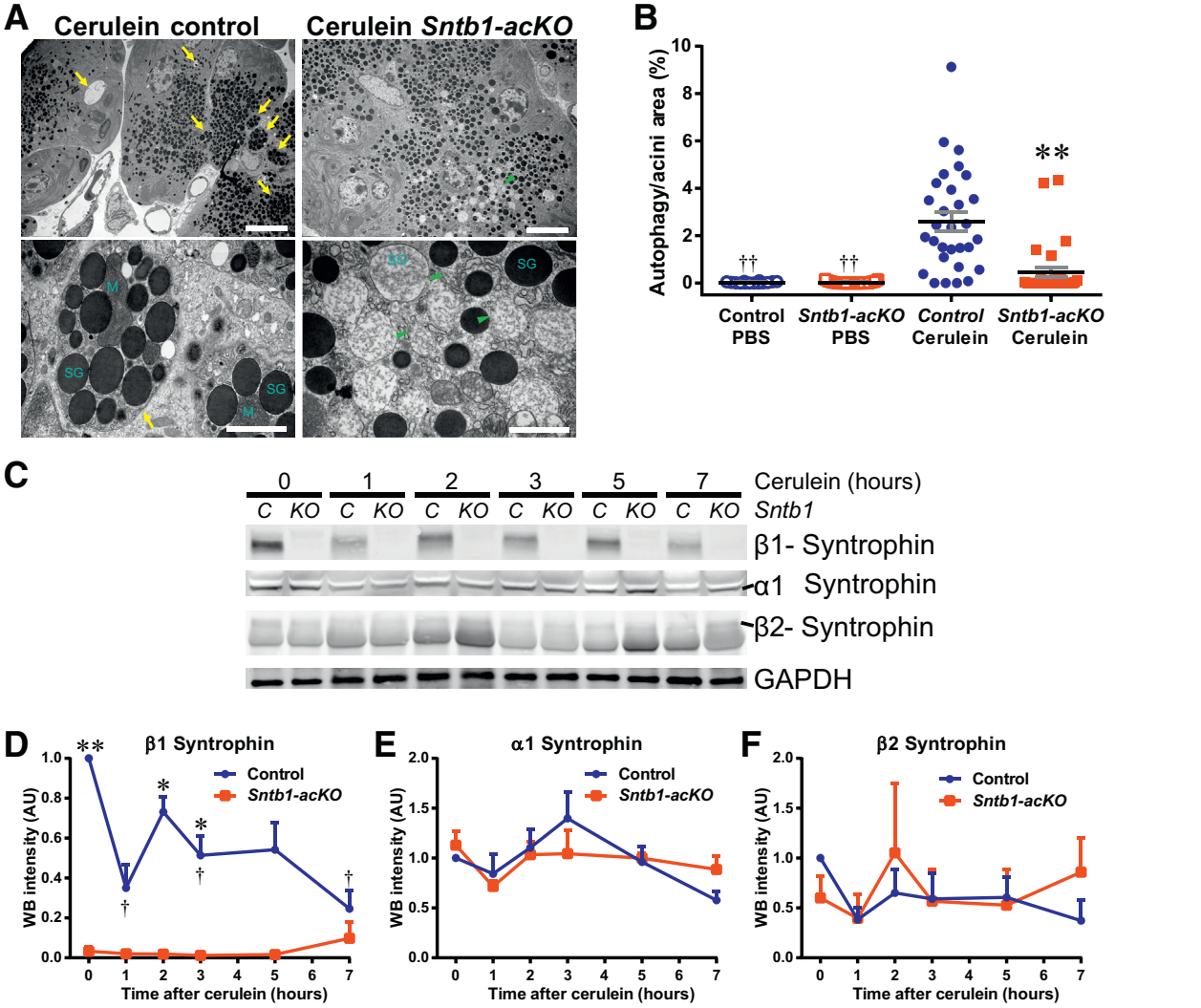

Figure 4 Diminished pancreatic autophagy in cerulein-treated *Sntb1-acKO* mice. **A** and **B:** Pancreata of mice after four hourly injections of cerulein were subjected to transmission electron microscopy. **A:** Representative images of pancreatic acini. **Arrows** indicate examples of autophagy featured by the double-membrane vesicles containing cell organelles, such as mitochondria (M) and secretory granules (SGs); **arrowheads**, examples of secretory granules with disrupted single-membrane and leaked content. **B:** Quantitation of autophagy area, normalized against total area of acini. Fields of 1.4 to 2.7 $\times$ 10^3 μm^2 acini were measured. **C**—**F:** Western blot (WB) analysis of syntrophins with mouse pancreata after 0, 1, 2, 3, 5, and 7 hourly injections of cerulein. **C:** Representative blots. **D**—**F:** Intensity volumes of β1 (**D**), α1 (**E**), and β2 (**F**) blots are quantitated and normalized against glyceraldehyde-3-phosphate dehydrogenase (GAPDH). Data are expressed as means ± SEM (**B** and **D**—**F**). $n = 14$ [**B**, phosphate-buffered saline (PBS)—treated control]; $n = 19$ (**B**, PBS-treated *Sntb1-acKO*); $n = 30$ (**B**, cerulein-treated control); $n = 31$ (**B**, cerulein-treated *Sntb1-acKO*); $n = 2$ or 3 mice per condition (**D**—**F**). $^*P < 0.05$, $^{**}P < 0.01$ *Sntb1-acKO* versus control mice; $^{\dagger}P < 0.05$ versus 0 hours after injection; $^{\dagger\dagger}P < 0.01$ cerulein versus PBS treatment. Scale bars: 2 μm (**A**, **top row**); 0.4 μm (**A**, **bottom row**). AU, arbitrary unit; C, control; KO, Sntb1-acKO.

reduction, followed by an immediate recovery in protein levels (Figure 5, A and C). In contrast to ATG9A, p62 proteins are further accumulated beyond the starting levels, and this accumulation is significantly faster in the *Sntb1-acKO* mice than in the controls. The acute decrease in ATG9A and p62 proteins may reflect the insult from the autoactivated digestive enzymes, and the following recovery may be induced by autophagic signaling. The excessive accumulation of p62 in *Sntb1-acKO* mice is consistent with their deficiencies in autophagosome and autolysosome formation (Figure 4, A and B, and Supplemental Figure S3) and the subsequent autophagic degradation. Significant changes were not observed in LC3-II, the autophagosome membrane protein, and its precursor LC3-I, by using Western blot analysis (Figure 5, A and D). However, immunofluorescence reveals a remarkable abnormality of LC3 distribution in *Sntb1-acKO* pancreas (Figure 5E). In the absence of β1 syntrophin, LC3 signals are more concentrated in the basolateral perinuclear regions of the acinar cells, rendering much fewer LC3-positive puncta in the apical region. The latter is consistent with the autophagosome depletion in *Sntb1-acKO* mice.

To test whether autolysosome formation plays a role in the autophagy deficiency in *Sntb1-acKO* mice, chloroquine, a lysosomal inhibitor, was administered to the mice

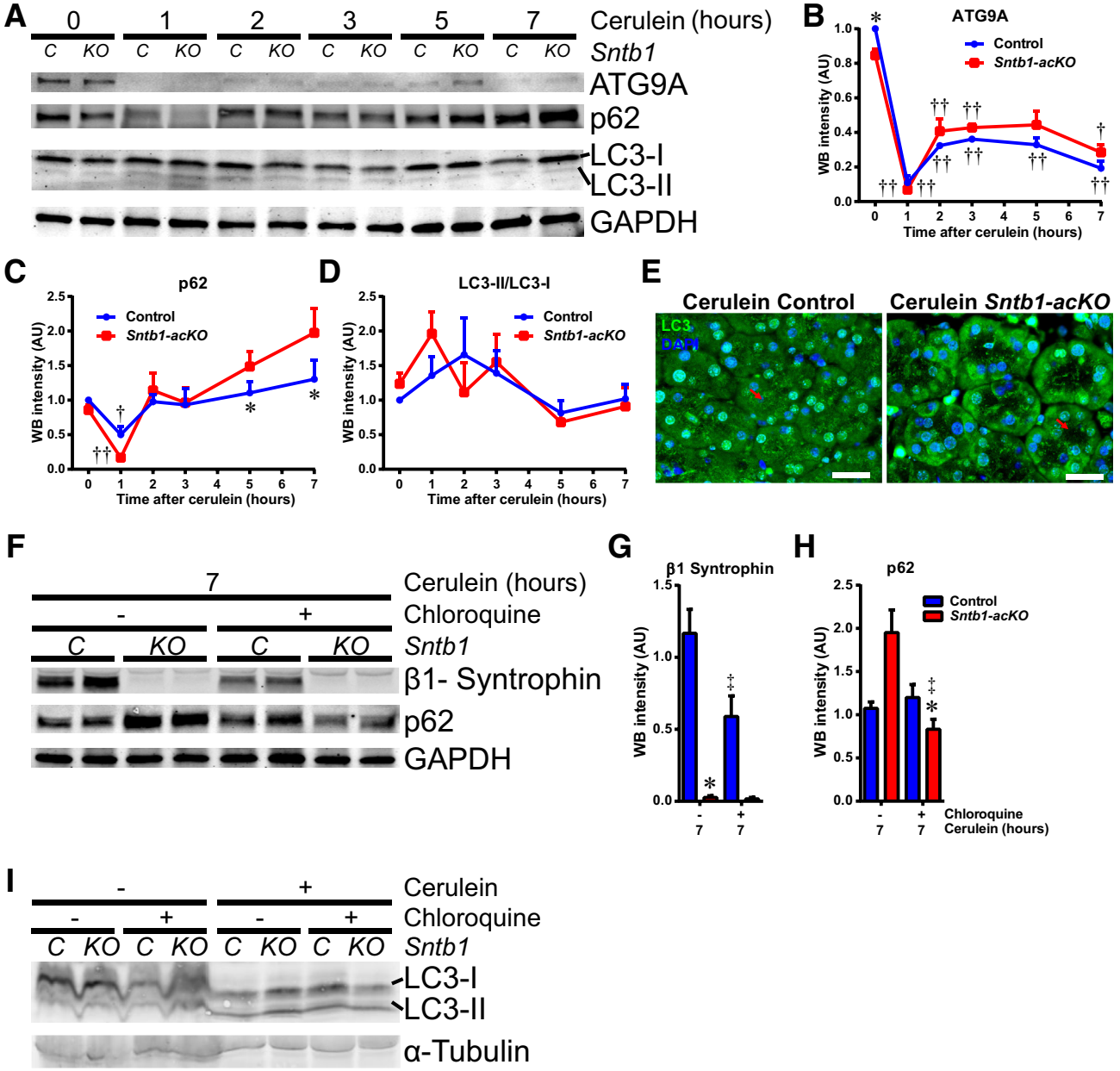

Figure 5 β1 Syntrophin modulates autophagy proteins during cerulein-induced acute pancreatitis. **A**–**D:** Western blot analysis of autophagy marker proteins with mouse pancreata after 0, 1, 2, 3, 5, and 7 hourly injections of cerulein. **A:** Representative blots. LC3-I and LC3-II duplex bands are indicated with lines. **B** and **C:** Intensity volumes of ATG9A (**B**) and p62 (**C**) blots are quantitated and normalized against glyceraldehyde-3-phosphate dehydrogenase (GAPDH). **D:** LC3-II blots are quantitated and normalized against LC3-I. **E:** Representative immunofluorescence of LC3 (green) counterstained with DAPI (blue). **Arrows** indicate apical region of acinar cells. **F**–**I:** *Sntb1-acKO* and control mice were subjected to seven hourly injections of cerulein or vehicle (-) and one injection of chloroquine or vehicle (-) 1.5 hours before sacrifice (ie, between the sixth and seventh cerulein or vehicle injections). Pancreata were subjected to Western blot (WB) analysis of autophagy modulators. **F:** Representative blots. **G** and **H:** Intensity volumes of β1 syntrophin (**G**) and p62 (**H**) blots are quantitated and normalized against GAPDH. **I:** Representative blots of LC3 proteins. LC3-I and LC3-II duplex bands are indicated with lines. Data are expressed as means ± SEM (**C**, **D**, **G**, and **H**). $n = 3$ mice per condition (**D**, **G**, and **H**). $^{*}P < 0.05$ for *Sntb1-acKO* versus control mice; $^{\dagger}P < 0.05$, $^{\dagger\dagger}P < 0.01$ versus time 0 after injection; $^{\ddagger}P < 0.05$ for chloroquine versus vehicle. Scale bars = 30 μm (**E**). AU, arbitrary unit; C, control; KO, Sntb1-acKO.

developing experimental acute pancreatitis. With chloroquine treatment, β1 syntrophin is further reduced in the control mice (Figure 5, F and G). In contrast, p62 shows a minimal change in controls, but a significant reduction in *Sntb1-acKO* mice (Figure 5, F and H). Chloroquine does not change LC3-II levels in vehicle-treated groups. On both cerulein and chloroquine treatment, LC3-II levels are increased in controls, but unaltered in *Sntb1-acKO* mice (Figure 5I). Considering the scarcity of both autophagosomes and autolysosomes in *Sntb1* knockout acinar cells, the step of lysosome-autophagosome fusion is unlikely playing an important role there.

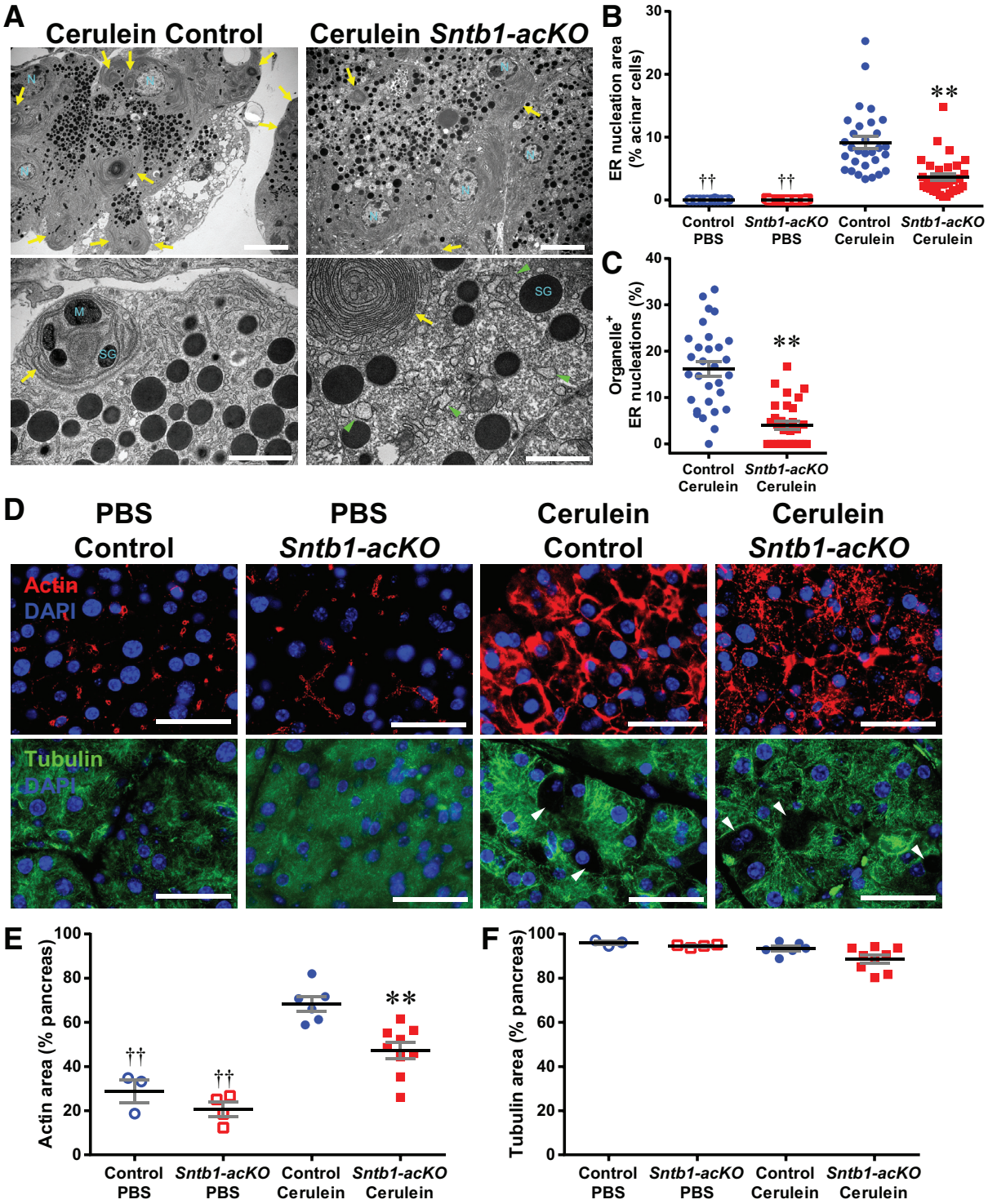

Figure 6 Impaired endoplasmic reticulum (ER) nucleation and actin assembly in *Sntb1-acKO* mice. **A**–**C:** Pancreata of mice after four hourly injections of phosphate-buffered saline (PBS) or cerulein were subjected to transmission electron microscopy. **A:** Representative images of acinar cells with ER nucleation. **Yellow arrows** indicate examples of ER nucleation; **green arrowheads**, examples of dilated ER. **B:** Quantitation of ER nucleation area, normalized against total area of acini. **C:** Percentages of ER nucleation containing cell organelles. Fields of 1.4 to 2.7 $\times$ 10^3 μm^2 acini were measured. **D**–**F:** Pancreas sections of mice after seven hourly injections of PBS or cerulein were subjected to immunofluorescence of β-actin or α-tubulin. **D:** Representative images of β-actin (red) and α-tubulin (green) counterstained with DAPI (blue). **Arrowheads** indicate necrotic acinar cells losing tubulin signal. **E** and **F:** Quantitation of β-actin (**E**) and α-tubulin (**F**) positive areas, normalized against the area of pancreas. Dots represent individual mice. Data are expressed as means ± SEM (**B**, **C**, **E**, and **F**). n = 14 (**C**, PBS-treated control); n = 19 (**C**, PBS-treated *Sntb1-acKO*); n = 30 (**C**, cerulein-treated control); n = 31 (**C**, cerulein-treated *Sntb1-acKO*); n = 3 (**E** and **F**, PBS-treated control); n = 4 (**E** and **F**, PBS-treated *Sntb1-acKO*); n = 6 (**E** and **F**, cerulein-treated control); n = 9 (**E** and **F**, cerulein-treated *Sntb1-acKO*). $^{**}P < 0.01$ *Sntb1-acKO* versus control mice; $^{\dagger\dagger}P < 0.01$ cerulein versus PBS treatment. Scale bars: 2 μm (**A**, **top row**); 0.4 μm (**A**, **bottom row**); 40 μm (**D**). M, mitochondrion; N, nucleus; SG, secretory granule.

β1 Syntrophin Regulates Actin Distribution and ER Nucleation in Pancreatic Acinar Cells during Cerulein-Induced Acute Pancreatitis

The deficiencies in both autophagosomes and autolysosomes suggest that some early steps of autophagy formation are blocked in the absence of β1 syntrophin. In control acinar cells, cerulein induces abundant ER nucleation (ie, structures of high-curvature ER membranes, indicating autophagy initiation) (Figure 6, A and B). Areas of ER nucleation are significantly decreased in *Sntb1-acKO* mice (3.6% ± 0.5% versus 9.1% ± 0.9%; $P = 4.9 \times 10^{-6}$). Furthermore, a significantly lower portion of the *Sntb1-acKO* ER nucleations contain other intracellular organelles (eg, mitochondria and secretory granules) than the controls (4.0% ± 0.9% versus 16.2% ± 1.6%; $P = 2.3 \times 10^{-8}$) (Figure 6, A and C). These findings support an essential role of β1 syntrophin in autophagy initiation. Interestingly, widespread dilated ER was also observed in the *Sntb1* knockout acinar cells but not in controls (Figure 6A), suggesting ER stress associated with the massive leakage of digestive enzymes (Figure 4A).

As part of the cytoskeleton, actin filaments are physically linked to the syntrophin complex via dystrophin,[5] and they are essential for maintenance of ER curvature and the subsequent formation of omegasomes and phagophores.[22] The intracellular distribution of actin was examined by immunofluorescence (Figure 6, D and E). Cerulein treatment dramatically increases actin signals in both genotypes. However, the perinuclear distribution of actin is much more prominent in controls than in *Sntb1-acKO* mice, suggesting strong actin assembly in the ER-enriched area, and consistent with the abundant ER nucleations (Figure 6, A and B). The dispersed actin signal in cerulein-treated *Sntb1-acKO* mice suggest defects in actin network formation, consistent with the diminished ER nucleations. Such differences are not observed with tubulin (Figure 6, D and F), supporting a model in which β1 syntrophin regulates specifically the actin network to initiate autophagy.

Discussion

The syntrophin family of proteins binds and regulates dystrophin, the critical bridge protein between cytoskeleton and transmembrane glycoproteins.[23] Although the function of dystrophin has been well studied in muscle and neurons, much less is known about syntrophins. Among the five members of the syntrophin family, α1 syntrophin has been studied the most as a pleiotropic adaptor for neuronal nitric oxide synthase,[24] Na^+ channels,[25] Kir4.1 K^+ channel,[26] and F-actin.[8] The knockout mouse model of α1 syntrophin showed diminished acetylcholinesterases, postsynaptic acetylcholine receptors, and utrophin in neuromuscular junctions,[27] as well as depleted aquaporin-4 water channel levels in skeletal muscle.[28] Interestingly, normal expression—but a reversed polarity of subcellular localization of aquaporin-4—was observed in α1 syntrophin–ablated mouse brains and muscle tissues.[28] The current study characterizes the physiological roles of β1 syntrophin, the least characterized member of the family, in the endocrine and exocrine pancreas. Although the loss of β1 syntrophin appears to have no impact on the ultrastructure and function of insulin-producing β cells, it significantly reduces CFTR expression in the exocrine acinar cells and dilates acinar lumina. The more pronounced phenotype in acinar cells is likely due to much higher expression levels in the exocrine pancreas compared with the endocrine pancreas under normal conditions. Of clinical significance, β1 syntrophin–deficient acinar cells are more susceptible to cerulein-induced acute pancreatitis, associated with a failure to induce autophagy, resulting in intracellular leakage of secretory granules with the highly pronecrotic digestive enzymes. The transient increase in caspase-3 activity does not prevent the exacerbated necrosis. Future studies with other highly reproducible mouse models of acute pancreatitis, such as L-arginine injection and the choline-deficient, ethionine-supplemented diet,[29] will further elucidate how β1 syntrophin protects against the progression of acute pancreatitis.

It is well established in cystic fibrosis patients that the CFTR defect can result in pancreatic duct dilation via disruption of ion exchange, increase in fluid absorption, and accumulation of ductal mucus.[20] With β1 syntrophin ablation exclusively in pancreatic acinar cells, CFTR reduction was observed in both acinar and ductal cells. One plausible explanation could be trafficking of CFTR-containing membranes between these two cell types, although the regulatory link between β1 syntrophin and CFTR awaits further investigation. Cystic fibrosis patients also present insufficient secretion of digestive enzymes from exocrine pancreas and chronic pancreatitis. However, these pathologic changes are not evident in our mouse model. Future studies with aged *Sntb1-acKO* mice are warranted to test the pathogenesis of pancreatic insufficiency, fibrosis, and chronic pancreatitis.

These results provide insights for a better understanding of the molecular events of cerulein-induced acute pancreatitis and how this process intertwines with autophagy. Autoactivation of digestive enzymes results in an acute degradation of cytoplasmic proteins, such as β1 syntrophin, ATG9A, and p62. In response to the digestive enzyme crisis, autophagy is induced, as demonstrated by up-regulation of these key proteins immediately after the initial ablation. In the control mice, in which the autophagic activity is relatively intact, digestive enzyme granules are well contained in autophagosomes and then degraded in autolysosomes. If the formation of autolysosomes from autophagosome-lysosome fusion is inhibited by a lysosomal inhibitor (eg, chloroquine), the digestive enzymes may eventually breach the autophagosome barrier and ignite a burst of cellular degradation, to which β1 syntrophin is highly susceptible and the membrane-anchored LC3-II is more resistant than p62. In the acinar cells lacking β1 syntrophin, autophagosome formation is predominantly

halted at the initial steps (ie, actin-mediated budding of omegasomes and phagophores from the ER membrane). Hence, the LC3-II anchored membranes are stuck in the ER-enriched basolateral perinuclear region, leaving the apical region scarce of autophagosomes and autolysosomes. In this case, LC3-II is not sensitive to the lysosomal inhibitors because most LC3 proteins are not processed to either autophagosomes or autolysosomes. The unantagonized digestive enzyme crisis promotes extra accumulation of p62, which is abolished by lysosomal inhibition.

Evidence is emerging that the actin cytoskeleton is an integral player during the process of autophagy. Back in 1992, Aplin and colleagues[30] suggested that actin microfilaments are required for autophagosome formation, whereas tubulin microtubules enable the delivery of lysosomal enzymes to form autolysosomes. The branching actin network functions physically to stabilize and expand the curvature of the ER membrane.[31] When the autophagosomes become mature, they are propelled away from the ER by actin filaments via a comet tail mechanism.[32] Actin was also shown to facilitate the generation of phosphatidyl-inositol-3-phosphate required for autophagosome formation. RhoA and Rac1, the GTPase regulators of actin remodeling, regulate starvation-induced autophagy.[33] On the other hand, actin expression may depend on ATG7, an upstream inducer of autophagy.[34] Consistent with these reports, in β1 syntrophin knockout acinar cells after cerulein treatment, defective actin assembly was observed, associated with a marked reduction in ER nucleations, autophagosomes, and autolysosomes.

The role of autophagy in the pathophysiology of acute pancreatitis needs further characterization. Multiple studies reported induction of autophagy in acute pancreatitis animal models.[35,36] As an adaptive response to the pathologic insults, autophagic flux may eventually be impaired due to lysosomal dysfunction, which aggravates trypsinogen autoactivation instead.[36,37] On the other hand, these data suggest that a major inhibition of autophagosome formation also exacerbates acute pancreatitis. Therefore, autophagy may be initiated in acinar cells to protect against acute pancreatitis. Stabilizing autophagic flux and function may be a viable and successful strategy to combat acute pancreatitis as well as other autophagy-related diseases, with β1 syntrophin as a promising target.

Acknowledgments

We thank Dr. Rajat Singh (Albert Einstein College of Medicine) for the insightful comments, Kristen Wertz for technical assistance, the University of Texas Southwestern Medical Center (UTSW) Mouse Phenotyping Core for metabolic assays, and the UTSW Electron Microscopy Core and Molecular Pathology Core for tissue embedding and processing.

R.Y. planned and conducted experiments, acquired and analyzed data, and wrote the manuscript; T.O., P.-G.B., and V.E. planned and conducted experiments and acquired and analyzed data; C.M.K. and R.A.B. provided reagents; P.E.S. conceptualized the studies, designed experiments, analyzed data, and wrote the manuscript.

Supplemental Data

Supplemental material for this article can be found at *https://doi.org/10.1016/j.ajpath.2019.01.002*.

References

1. Lankisch PG, Apte M, Banks PA: Acute pancreatitis. Lancet 2015, 386:85−96
2. Hyun JJ, Lee HS: Experimental models of pancreatitis. Clin Endosc 2014, 47:212−216
3. Bhat HF, Adams ME, Khanday FA: Syntrophin proteins as Santa Claus: role(s) in cell signal transduction. Cell Mol Life Sci 2013, 70: 2533−2554
4. Alessi A, Bragg AD, Percival JM, Yoo J, Albrecht DE, Froehner SC, Adams ME: γ-Syntrophin scaffolding is spatially and functionally distinct from that of the α/β syntrophins. Exp Cell Res 2006, 312: 3084−3095
5. Fairclough RJ, Wood MJ, Davies KE: Therapy for Duchenne muscular dystrophy: renewed optimism from genetic approaches. Nat Rev Genet 2013, 14:373−378
6. Gavillet B, Rougier J-S, Domenighetti AA, Behar R, Boixel C, Ruchat P, Lehr H-A, Pedrazzini T, Abriel H: Cardiac sodium channel $Na_v1.5$ is regulated by a multiprotein complex composed of syntrophins and dystrophin. Circ Res 2006, 99:407−414
7. Leonoudakis D, Conti LR, Anderson S, Radeke CM, McGuire LMM, Adams ME, Froehner SC, Yates JR, Vandenberg CA: Protein trafficking and anchoring complexes revealed by proteomic analysis of inward rectifier potassium channel (Kir2.x)-associated proteins. J Biol Chem 2004, 279:22331−22346
8. Iwata Y, Sampaolesi M, Shigekawa M, Wakabayashi S: Syntrophin is an actin-binding protein the cellular localization of which is regulated through cytoskeletal reorganization in skeletal muscle cells. Eur J Cell Biol 2004, 83:555−565
9. Ort T, Voronov S, Guo J, Zawalich K, Froehner SC, Zawalich W, Solimena M: Dephosphorylation of β2-syntrophin and Ca2+/μ-calpain-mediated cleavage of ICA512 upon stimulation of insulin secretion. EMBO J 2001, 20:4013−4023
10. Schubert S, Knoch K-P, Ouwendijk J, Mohammed S, Bodrov Y, Jäger M, Altkrüger A, Wegbrod C, Adams ME, Kim Y, Froehner SC, Jensen ON, Kalaidzidis Y, Solimena M: β2-Syntrophin is a Cdk5 substrate that restrains the motility of insulin secretory granules. PLoS One 2010, 5:e12929
11. Kusminski CM, Chen S, Ye R, Sun K, Wang QA, Spurgin SB, Sanders PE, Brozinick JT, Geldenhuys WJ, Li WH, Unger RH, Scherer PE: MitoNEET-parkin effects in pancreatic α- and β-cells, cellular survival, and intrainsular cross talk. Diabetes 2016, 65:1534−1555
12. Ye R, Wang M, Wang QA, Spurgin SB, Wang ZV, Sun K, Scherer PE: Autonomous interconversion between adult pancreatic α-cells and β-cells after differential metabolic challenges. Mol Metab 2016, 5: 437−448
13. Ye R, Holland WL, Gordillo R, Wang M, Wang QA, Shao M, Morley TS, Gupta RK, Stahl A, Scherer PE: Adiponectin is essential for lipid homeostasis and survival under insulin deficiency and promotes β-cell regeneration. eLife 2014, 3:e03851
14. Ye R, Mareninova OA, Barron E, Wang M, Hinton DR, Pandol SJ, Lee AS: Grp78 heterozygosity regulates chaperone balance in exocrine pancreas with differential response to cerulein-induced acute pancreatitis. Am J Pathol 2010, 177:2827−2836

15. Ye R, Wang M, Wang QA, Scherer PE: Adiponectin-mediated antilipotoxic effects in regenerating pancreatic islets. Endocrinology 2015, 156:2019−2028
16. Williams JA: Isolation of rodent pancreatic acinar cells and acini by collagenase digestion. Pancreapedia 2010, doi:10.3998/panc.2010.18
17. Skarnes WC, Rosen B, West AP, Koutsourakis M, Bushell W, Iyer V, Mujica AO, Thomas M, Harrow J, Cox T, Jackson D, Severin J, Biggs P, Fu J, Nefedov M, de Jong PJ, Stewart AF, Bradley A: A conditional knockout resource for the genome-wide study of mouse gene function. Nature 2011, 474:337−342
18. Magnuson MA, Osipovich AB: Pancreas-specific Cre driver lines and considerations for their prudent use. Cell Metab 2013, 18:9−20
19. Frizzell RA, Hanrahan JW: Physiology of epithelial chloride and fluid secretion. Cold Spring Harb Perspect Med 2012, 2:a009563
20. Wilschanski M, Novak I: The cystic fibrosis of exocrine pancreas. Cold Spring Harb Perspect Med 2013, 3:a009746
21. Birgisdottir ÅB, Lamark T, Johansen T: The LIR motif−crucial for selective autophagy. J Cell Sci 2013, 126:3237−3247
22. Kast DJ, Dominguez R: The cytoskeleton-autophagy connection. Curr Biol 2017, 27:R318−R326
23. Gao Q, McNally EM: The Dystrophin complex: structure, function and implications for therapy. Compr Physiol 2015, 5:1223−1239
24. Hashida-Okumura A, Okumura N, Iwamatsu A, Buijs RM, Romijn HJ, Nagai K: Interaction of neuronal nitric-oxide synthase with α1-syntrophin in rat brain. J Biol Chem 1999, 274:11736−11741
25. Gee SH, Madhavan R, Levinson SR, Caldwell JH, Sealock R, Froehner SC: Interaction of muscle and brain sodium channels with multiple members of the syntrophin family of dystrophin-associated proteins. J Neurosci 1998, 18:128−137
26. Connors NC, Adams ME, Froehner SC, Kofuji P: The potassium channel Kir4.1 associates with the dystrophin-glycoprotein complex via α-syntrophin in glia. J Biol Chem 2004, 279:28387−28392
27. Adams ME, Kramarcy N, Krall SP, Rossi SG, Rotundo RL, Sealock R, Froehner SC: Absence of α-syntrophin leads to structurally aberrant neuromuscular synapses deficient in utrophin. J Cell Biol 2000, 150:1385−1398
28. Neely JD, Amiry-Moghaddam M, Ottersen OP, Froehner SC, Agre P, Adams ME: Syntrophin-dependent expression and localization of Aquaporin-4 water channel protein. Proc Natl Acad Sci U S A 2001, 98:14108−14113
29. Su KH, Cuthbertson C, Christophi C: Review of experimental animal models of acute pancreatitis. HPB (Oxford) 2006, 8:264−286
30. Aplin A, Jasionowski T, Tuttle DL, Lenk SE, Dunn WA: Cytoskeletal elements are required for the formation and maturation of autophagic vacuoles. J Cell Physiol 1992, 152:458−466
31. Zientara-Rytter K, Subramani S: Role of actin in shaping autophagosomes. Autophagy 2016, 12:2512−2515
32. Kast David J, Zajac Allison L, Holzbaur Erika LF, Ostap EM, Dominguez R: WHAMM directs the Arp2/3 complex to the ER for autophagosome biogenesis through an actin comet tail mechanism. Curr Biol 2015, 25:1791−1797
33. Aguilera MO, Berón W, Colombo MI: The actin cytoskeleton participates in the early events of autophagosome formation upon starvation induced autophagy. Autophagy 2012, 8:1590−1603
34. Zhuo C, Ji Y, Chen Z, Kitazato K, Xiang Y, Zhong M, Wang Q, Pei Y, Ju H, Wang Y: Proteomics analysis of autophagy-deficient Atg7−/− MEFs reveals a close relationship between F-actin and autophagy. Biochem Biophys Res Commun 2013, 437:482−488
35. Zhang L, Zhang J, Shea K, Xu L, Tobin G, Knapton A, Sharron S, Rouse R: Autophagy in pancreatic acinar cells in caerulein-treated mice: immunolocalization of related proteins and their potential as markers of pancreatitis. Toxicol Pathol 2014, 42:435−457
36. Mareninova OA, Hermann K, French SW, O'Konski MS, Pandol SJ, Webster P, Erickson AH, Katunuma N, Gorelick FS, Gukovsky I, Gukovskaya AS: Impaired autophagic flux mediates acinar cell vacuole formation and trypsinogen activation in rodent models of acute pancreatitis. J Clin Invest 2009, 119:3340−3355
37. Hashimoto D, Ohmuraya M, Hirota M, Yamamoto A, Suyama K, Ida S, Okumura Y, Takahashi E, Kido H, Araki K, Baba H, Mizushima N, Yamamura K-I: Involvement of autophagy in trypsinogen activation within the pancreatic acinar cells. J Cell Biol 2008, 181:1065−1072